Opto-Electronic Advances

CN 51–1781/TN ISSN 2096–4579 (Print) ISSN 2097–3993 (Online)

High-efficiency RGB achromatic liquid crystal diffractive optical elements

Yuqiang Ding, Xiaojin Huang, Yongziyan Ma, Yan Li and Shin-Tson Wu

Citation: Ding YQ, Huang XJ, Ma YZY, et al. High-efficiency RGB achromatic liquid crystal diffractive optical elements. *Opto-Electron Adv* **8**, 240181(2025).

https://doi.org/10.29026/oea.2025.240181

Received: 1 August 2024; Accepted: 29 October 2024; Published online: 7 January 2025

Opto-Electronic Advances

Article

March 2025, Vol. 8, No. 3

DOI: 10.29026/oea.2025.240181 CSTR: 32247.14.oea.2025.240181

High-efficiency RGB achromatic liquid crystal diffractive optical elements

Yuqiang Ding[1†], Xiaojin Huang[2†], Yongziyan Ma[1], Yan Li[2*] and Shin-Tson Wu[1*]

Liquid crystal Pacharatnam-Berry phase optical elements (PBOEs) have found promising applications in augmented reality and virtual reality because of their slim formfactor, lightweight, and high optical efficiency. However, chromatic aberration remains a serious longstanding problem for diffractive optics, hindering their broader adoption. To overcome the chromatic aberrations for red, green and blue (RGB) light sources, in this paper, we propose a counterintuitive multi-twist structure to achieve narrowband PBOEs without crosstalk, which plays a vital role to eliminate the chromatic aberration. The performance of our designed and fabricated narrowband Pacharatnam-Berry lenses (PBLs) aligns well with our simulation results. Furthermore, in a feasibility demonstration experiment using a laser projector, our proposed PBL system indeed exhibits a diminished chromatic aberration as compared to a broadband PBL. Additionally, polarization raytracing is implemented to demonstrate the versatility of the multi-twist structure for designing any RGB wavelengths with high contrast ratios. This analysis explores the feasibility of using RGB laser lines and quantum dot light-emitting diodes. Overall, our approach enables high optical efficiency, low fabrication complexity, and high degree of design freedom to accommodate any liquid crystal material and RGB light sources, holding immense potential for widespread applications of achromatic PBOEs.

Keywords: achromatic diffractive optical elements; Pacharatnam-Berry phase optical elements; liquid crystal planar optics; near-eye displays

Ding YQ, Huang XJ, Ma YZY et al. High-efficiency RGB achromatic liquid crystal diffractive optical elements. *Opto-Electron Adv* **8**, 240181 (2025).

Introduction

Augmented reality (AR) and virtual reality (VR) have expanded our perceptual horizons and ushered in deeper human-digital interactions that transcend the restraints of traditional flat panel displays. This evolution has unlocked a realm of exciting new possibilities, encompassing the metaverse, digital twins, and spatial computing, all of which have found widespread applications in diverse fields such as smart education and training, healthcare, navigation, gaming, entertainment, and smart manufacturing.

For AR and VR to become truly wearable, there is a pressing need for compact and stylish formfactor, lightweight, and low power consumption. To achieve these objectives, extensive efforts have been devoted to designing novel optical elements and system configurations[1–5]. Among these endeavors, liquid crystal (LC)-based Pacharatnam-Berry phase optical elements

[1]College of Optics and Photonics, University of Central Florida, Orlando, FL 32816, USA; [2]Department of Electronic Engineering, Shanghai Jiao Tong University, Shanghai 200240, China.

[†]These authors contributed equally to this work.

*Correspondence: Y Li, E-mail: yan.li@sjtu.edu.cn; ST Wu, E-mail: swu@creol.ucf.edu

Received: 1 August 2024; Accepted: 29 October 2024; Published online: 7 January 2025

(PBOEs)[6,7] (also called geometric phase) have emerged as a key enabler for compact and lightweight optical systems because of their ultrathin formfactor, nearly 100% diffraction efficiency, strong polarization selectivity, dynamic switching capability, simple fabrication process, and low cost.

While LC-based PBOEs can significantly reduce the formfactor and enhance the design flexibility, chromatic aberration has been a longstanding problem for these diffractive optics. A straightforward way to suppress chromatic aberration is to laminate a PBOE film to a refractive lens due to their opposite dispersion behaviors[8–10]. For instance, the material dispersion of a Fresnel lens can be used to counteract the chromatic aberration caused by the PBOEs[8]. Although this approach greatly reduces the chromatic aberration, the overall formfactor remains bulky and heavy resulting from the refractive lens, compared to that using PBOEs alone.

To tackle the chromatic aberration of PBOEs without compromising formfactor and weight, planar optical elements are proven to be effective. One method is to use switchable PBOEs[11,12] that can modulate the effective phase retardation, allowing them to work with different colors in separate frames. For example, to eliminate chromatic aberration, a color sequential display is implemented to match the frame rate of the switchable PBOEs. In so doing, the chromatic aberration for red, green, and blue (RGB) light sources could be suppressed because they operate independently in different frames. However, this approach demands a high frame rate (≥720 Hz) for both PBOEs and display panels, otherwise, color breakup will occur. Another method to correct chromatic aberration also involves modulating the displays, known as digital compensation. This approach significantly reduces the chromatic aberration by pre-processing images according to the chromatic aberration characteristics of the PBOEs, similar to the lens correction in photography[13]. However, the digital compensation method has its own limits. In a wearable AR/VR display, power consumption and thermal effects are critical issues due to the high memory and computation demands required for digital compensation, especially for a high-resolution-density display.

To alleviate the burden on displays, significant efforts have been directed toward improving PBOEs and other optical elements, such as waveplates and hologram films. One approach is to stack three RGB narrowband PBOEs together[14–16], with each one responsible for a different color. Another method is to combine PBOEs with another color-selective PBOEs, half-wave plate (HWP)[17,18] or holographic optical elements[19] to adjust the effective functionality for each color. For example, Luo, et al.[17] corrected the chromatic aberration in a broadband PBL by using a blue HWP in conjunction with a blue-red PBL. However, these achromatic systems suffer from compromised optical efficiency, limited design freedom for different wavelengths, and ghost images, which stem from limited narrowband performance, which leads to color crosstalk of the PBOEs or HWP. More specifically, a common approach to create the narrowband HWPs or PBOEs is to achieve high-order half-wave conditions[14,17]. Yet, limited by the birefringence (Δn) dispersion of liquid crystals[20], this method works well only for certain wavelengths. For example, a high-order blue HWP exhibits a 50% crosstalk at green light[17], causing a significant optical loss and ghost images. To avoid crosstalk, the blue light wavelength may be restricted to around 490 nm[14], which in turn limits the design flexibility. Engineering the dispersion of LC materials could mitigate this issue, but it requires substantial material synthesis efforts. Another approach involves using Solc filter-like structures[21] to achieve narrowband HWPs or PBOEs. However, fabricating multiple homogeneous LC layers on a single substrate for Solc filters is challenging. To address this, a new technique[15,22] to connect each homogeneous layer with an ultrathin twisted LC layer has been devised, ensuring that the optical axis of each homogeneous layer can have different azimuthal angles, thereby achieving narrowband performance. However, this method requires a relatively large $d\Delta n$(≈2.8 μm) LC film for each color; here d stands for the LC layer thickness. Such a process increases the fabrication complexity, making crosstalk more likely, and finally leading to a significant optical loss and ghost images.

To address the abovementioned issues, here we propose a counterintuitive method using a multi-twist structure to achieve achromatic PBOEs. More specifically, instead of realizing wide-view and broadband PBOEs[23–28], the multi-twist structure is designed and optimized using Rigorous Coupled-Wave Analysis (RCWA) to achieve narrowband PBOEs for any RGB light sources with minimal crosstalk. Based on the design, such narrowband PBLs with $f/\#$ =4 are fabricated and the experimental results align well with RCWA simulations. Besides, we also experimentally validate the achromatic performance of these narrowband PBLs using a laser

projector. The chromatic aberration is indeed dramatically suppressed, in comparison with a broadband PBL system. To further prove the design freedom of the multi-twist structure for choosing any RGB wavelengths with a high contrast ratio, polarization raytracing is conducted in OpticStudio to analyze the potential of our approach using a laser projector and quantum dot light-emitting diode (QD LED) sources. Overall, our proposed method provides a high optical efficiency, reduced fabrication complexity, and high degree of design freedom for any LC material and RGB light sources. Widespread applications of these new achromatic PBOEs are foreseeable.

Working principles

Unlike a refractive optics that relies on the optical path difference to create the desired phase pattern, LC-based PBOEs are composed of spatially patterned half-wave plates (HWPs) with liquid crystal axes oriented in various azimuthal directions[29–31] as Fig. 1(a) depicts. The phase modulation in these devices is directly related to the axis orientation, i.e., the LC azimuthal angle $\varphi(x,y)$. More specifically, the working principle can be explained using Jones matrices. First, the polarization state of a circularly polarized light can be expressed as[7]:

$$J_{\pm}=\frac{1}{\sqrt{2}}\begin{bmatrix}1\\ \pm \mathrm{i}\end{bmatrix}, \tag{1}$$

where J_+ and J_- represent the left-handed circular polarization (LCP) and right-handed circular polarization (RCP), respectively. When a circularly polarized light passing through a HWP with azimuthal angle φ, the output beam can be calculated as follows[7]:

$$\begin{aligned}J_{\mathrm{out}}^{'}&=R(-\varphi)*W(\phi)*R(\varphi)*\frac{1}{\sqrt{2}}\begin{bmatrix}1\\ \pm \mathrm{i}\end{bmatrix}\\&=\mathrm{e}^{\pm \mathrm{i}2\varphi}\frac{1}{\sqrt{2}}\begin{bmatrix}1\\ \mp \mathrm{i}\end{bmatrix},\end{aligned} \tag{2}$$

where R corresponds to the rotation matrix, W is the phase retardation matrix, and ϕ is the phase retardation of the HWP. As Eq. (2) indicates, an additional opposite phase delay of $\pm 2\varphi$ is introduced to the LCP and RCP light, respectively. By modulating the phase delay spatially, the resulting phase pattern can be configured as a grating, a lens, or any other hologram[32], depending on the design requirements. For example, if the PBOE is an lens (PBL) with a parabolic phase, then the spatial distribution of the LC director azimuthal angle $\varphi(x,y)$ follows a paraboloid function:

$$\varphi_L(x,y)=\frac{\pi}{\lambda f}(x^2+y^2), \tag{3}$$

where λ denotes the incident wavelength and f stands for the focal length of the PBL. Additionally, the circular polarization state of the outgoing beam is switched. For example, if the PBL is designed to function as a diverging lens for LCP, then it behaves as a converging lens for RCP. This dual functionality is due to the phase shift introduced by the PBL, which is dependent on the circular polarization state of the incident light. Thus, by carefully designing the azimuthal angle distribution $\varphi(x,y)$, a PBOE can be tailored to achieve the desired optical effect for a specific polarization state, enabling versatile applications in various optical systems.

However, the phase profile in Eq. (3) is wavelength dependent. Therefore, the focal length of the PBL will vary with the wavelength as follows:

$$\lambda_{\mathrm{R}}f_{\mathrm{R}}=\lambda_{\mathrm{G}}f_{\mathrm{G}}=\lambda_{\mathrm{B}}f_{\mathrm{B}}, \tag{4}$$

where $\lambda_{\mathrm{R}},\lambda_{\mathrm{G}}$,and λ_{B} represent the incident RGB wavelengths, and $f_{\mathrm{R}},f_{\mathrm{G}}$, and f_{B} are the corresponding focal lengths of the PBL. Based on Eq. (4), chromatic aberration arises in a PBL because the focal length varies with the wavelength, leading to different focal points for different colors, as illustrated in Fig. 1(b).

To mitigate or eliminate chromatic aberration, the

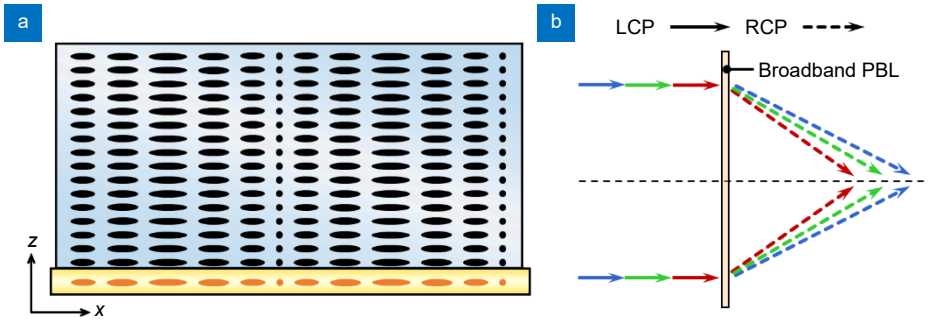

Fig. 1 | Working principles of PBOEs. (**a**) Planar LC structure of a general PBOE. (**b**) Chromatic aberration in a broadband PBL.

three PBLs can be specifically designed to match the RGB colors so that they have the same focal length. However, crosstalk between PBLs can cause serious light loss and ghost images because they must pass through the RGB colors simultaneously. To suppress crosstalk, these PBLs should have a narrow spectral bandwidth, i.e., each narrowband PBL only works for a single color, as Fig. 2(a–c) shows. For example, the PBL designed for red light should only focus the red light while not affecting the blue and green lights. In this way, chromatic aberration among the RGB colors can be eliminated, as shown in Fig. 2(d). To avoid crosstalk, here, we realize the narrowband spectra with the multi-twist structures shown in Fig. 2(e), where each layer has a different twist angle α_i and thickness d_i. By optimizing the thickness and twist angle of each layer to achieve different phase retardation for RGB colors, the narrowband spectrum without crosstalk among RGB light could be easily achieved. Besides, such a narrowband spectrum design can be extended to other patterns or holograms[32] since the essence of PBOEs is a spatially patterned HWP, as discussed earlier.

Results and discussion

To prove concept, we designed three multi-twist structures to achieve narrowband LC-based PBLs with central wavelengths of 445 nm, 520 nm, and 639 nm. Reactive mesogen RM257 with a birefringence of $\Delta n = 0.123 + 10990/\lambda^2$ was applied in simulations and experiments. By optimizing the thickness and twist angle of the multi-twist structures using Jones matrix, narrowband spectra for the RGB wavelengths are achieved, as Fig. 3(a–c) shows.

Based on the optimized twist angles and thicknesses of multi-twist structures listed in Table 1, we also fabricated the three narrowband PBLs. To correct the chromatic

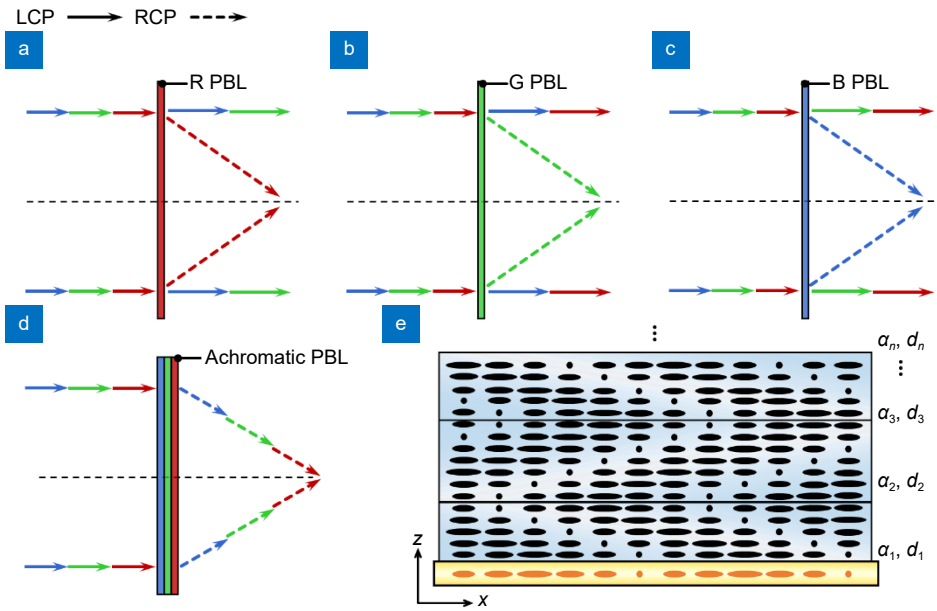

Fig. 2 | Working principles of the proposed achromatic PBL systems. Optical response of the incident RGB lights to (**a**) a red PBL, (**b**) a green PBL, (**c**) a blue PBL, and (**d**) a stacked RGB achromatic PBL. (**e**) LC structure for a multi-twist PBOE.

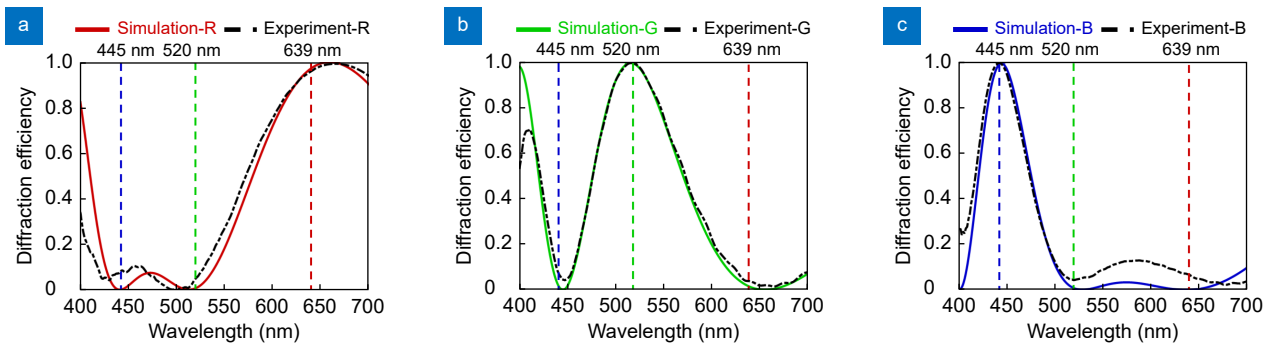

Fig. 3 | Spectral response of designed narrowband PBLs. Simulation and experimental spectrum of (**a**) red PBL, (**b**) green PBL, and (**c**) blue PBL.

aberration, it is essential for the RGB PBLs to have the same focal lengths at RGB colors. Here, we used a Mach-Zehnder Interferometer (MZI) to obtain the desired focal lengths for the RGB PBLs by recording the interference patterns on a photoalignment layer (PAL) sensitive to the linear polarization states of the incident beams.

More specifically, Fig. 4(a) illustrates the optical setup for the exposure process in detail. It begins with a collimated laser beam (λ=457 nm) that is initially split into two beams using a polarization beam splitter (PBS). These two beams are then converted to opposite circular polarization states (LCP and RCP) using the quarter-wave plate (QWP) in each arm. The RCP beam, which carries a lens phase pattern $\phi_L(x,y)$, is recombined with the LCP beam, which has no phase pattern, at the sample by the beam splitter (BS).

This setup creates interference that can be expressed using the Jones matrix representation as follows[7]:

$$J = \frac{1}{\sqrt{2}}\begin{bmatrix} 1 \\ -\mathrm{i} \end{bmatrix} \mathrm{e}^{\mathrm{i}\varphi_L(x,y)} + \frac{1}{\sqrt{2}}\begin{bmatrix} 1 \\ \mathrm{i} \end{bmatrix} = \begin{bmatrix} \cos\left(\dfrac{\varphi_L(x,y)}{2}\right) \\ \sin\left(\dfrac{\varphi_L(x,y)}{2}\right) \end{bmatrix} \mathrm{e}^{\mathrm{i}\frac{\varphi_L(x,y)}{2}} . \tag{5}$$

In most cases, the exposure wavelength differs from the operating wavelengths due to the absorption peak of our photoalignment material, which is situated in the blue or UV spectral region. Nevertheless, the PBOEs produced can effectively function for the green and red lights, depending on the design shown in Eq. (3). Therefore, by adjusting the focal length of the template lens in the MZI, as indicated in Table 2, the focal lengths of the RGB PBLs can be modulated to be the same.

The fabrication process of PBLs is depicted in Fig. 4(b). Initially, the azo dye SD1 photoalignment material was spin-coated onto a 0.7-mm-thick glass substrate. Subsequently, the PAL underwent exposure in the MZI using a 457 nm laser. After exposure, RM 257 was used to create uniform LC layers via spin coating. Additionally, substrates with LC layers were briefly placed on a hot plate immediately after spin coating to enhance alignment. Finally, the PBOEs were exposed to UV light for stabilization. Through multiple coating processes in the above with detailed recipes summarized in Table 3, the designed multi-twist PBLs were achieved as Fig. 4(c) shows. However, current RGB PBLs are fabricated on three separate substrates, which may introduce alignment issue. For practical applications, the three RGB PBLs should be fabricated on a single substrate with separated buffer layers as Fig. 4(d) depicts. Furthermore, a broadband PBL with a focal length of 87.8 mm at λ= 520 nm was also fabricated as a reference.

Achieving the correct thickness and twist angle for each layer requires the spectrum to match the simulation. Therefore, we placed the PBLs between two absorptive circular polarizers after each spin-coating to measure their spectral performance, as illustrated in Fig. 4(e). For example, the spectrum of the first-layer red PBL aligns very well with the simulation (Fig. 4(f)) once the spin-coating speed and concentration of the chiral dopant are optimized. After optimizing the concentration of chiral dopants and spin-coating parameters for each layer, the measured spectra, depicted as dashed lines in Fig. 2(a–c), closely align with the Jones matrix simulation except for a small deviation. This deviation mainly arises from the slight mismatch in the thickness and twist angle of each layer. Besides, the nonuniform surface flatness introduced by the spin-coating process can also contribute to these spectral deviations.

Additionally, we also investigated the chromatic aberration of the three narrowband PBLs compared to that of a single broadband PBL using a laser projector with four wavelengths of 445 nm, 515 nm, 523 nm, and 639 nm. As illustrated in Fig. 5(a), these three narrowband PBLs are positioned between the laser projector and the receiving screen to modulate the projected image. Due to the polarization selectivity of the PBLs, a circular polarizer is

Table 1 | Parameters of RGB narrowband PBLs.

	B PBL		G PBL		R PBL	
PBL layer	d_i (nm)	α_i (°)	d_i (nm)	α_i (°)	d_i (nm)	α_i (°)
1st	1839.1	26	1398.8	−20	1279.8	−30
2nd	1860.4	−104.9	1380.9	−37.2	1403.1	3.7
3rd	2103.7	−76	1440.7	5.8	1326.5	−40.1
4th	1974.3	33.2	1531.8	80.3	1546.7	10.3
5th	-	-	1202.8	32.1	1196.4	29.2

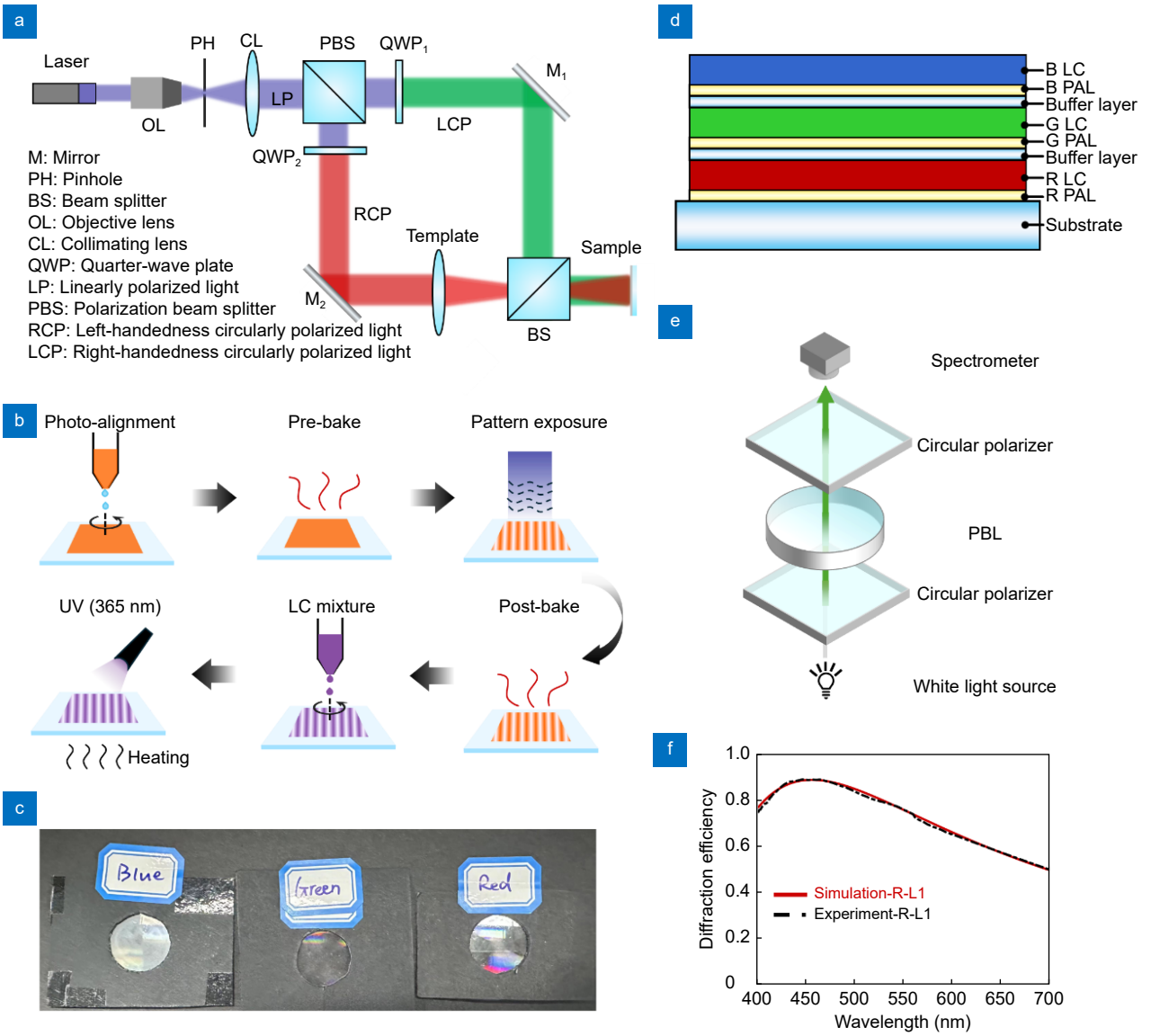

Fig. 4 | Experimental methods of PBOEs. **(a)** MZI for recording the phase profile. **(b)** Fabrication process of PBOEs. **(c)** Fabricated narrowband RGB PBLs samples. The diameter of each RGB sample is about 21.5 mm. **(d)** RGB PBLs on a common substrate with buffer layers. **(e)** Setup for characterizing the spectral response of PBOEs. **(f)** Measured spectral response of the first-layer LC in the red PBL, which consists of 5 layers in total.

Table 2 | Focal lengths of the template lens and PBLs.

	B PBL	G PBL	R PBL
Template focal length (mm)	85.0	100.0	122.1
PBL focal length (mm)	87.3	87.8	87.3

placed in front of the laser projector to convert the light into circular polarization. To suppress ghost images caused by imperfect spectra, an additional circular polarizer is positioned in front of the projection screen. Compared to the chromatic aberration induced by the broadband PBL shown in Fig. 5(b), each narrowband PBL only modulates the image of a single color, as Fig. 5(c–e) shows. Furthermore, by stacking three narrowband PBLs together, all the RGB beams from the laser projector are modulated and merged into a white image as shown in Fig. 5(f), which exhibits minimal chromatic aberration. Although there is still residual weak chromatic aberration in Fig. 5(f), it is mainly caused by the slight crosstalk as Fig. 2(a–c) depicts. In addition, the slightly

Table 3 | Materials and coating speed for the narrowband PBLs fabrication.

Sample	PBL layer	Solute	Solvent	Concentration（wt.%）	Coating speed (rpm)
B PBL	1st	RM257 (96.7%) R811 (0.3%) Irgacure 651 (3%)	Toluene	25	1200 (30s)
	2nd	RM257 (95.79%) S811 (1.21%) Irgacure 651 (3%)	Toluene	25	1650 (30s)
	3rd	RM257 (96.22%) S811 (0.78%) Irgacure 651 (3%)	Toluene	25	900 (30s)
	4th	RM257 (96.64%) R811 (0.36%) Irgacure 651 (3%)	Toluene	25	2000 (30s) 2200 (30s)
G PBL	1st	RM257 (96.68%) S811 (0.32%) Irgacure 651 (3%)	Toluene	20	2100 (30s)
	2nd	RM257 (96.42%) S811 (0.58%) Irgacure 651 (3%)	Toluene	20	1100 (30s)
	3rd	RM257 (96.91%) R811 (0.09%) Irgacure 651 (3%)	Toluene	20	1400 (30s)
	4th	RM257 (95.87%) R811 (1.13%) Irgacure 651 (3%)	Toluene	20	1000 (30s) 3000 (30s)
	5th	RM257 (96.43%) R811 (0.57%) Irgacure 651 (3%)	Toluene	20	1400 (30s)
R PBL	1st	RM257 (96.5%) S811 (0.5%) Irgacure 651 (3%)	Toluene	25	2350 (30s)
	2nd	RM257 (96.942%) R811 (0.058%) Irgacure 651 (3%)	Toluene	25	1400 (40s)
	3rd	RM257 (96.35%) S811 (0.65%) Irgacure 651 (3%)	Toluene	25	1600 (40s)
	4th	RM257 (96.854%) R811 (0.146%) Irgacure 651 (3%)	Toluene	25	1400 (40s)
	5th	RM257 (96.48%) S811 (0.52%) Irgacure 651 (3%)	Toluene	25	1400 (40s)

mismatched focal length of the RGB PBLs shown in Table 2 and the thickness of glass substrates (0.7 mm) also aggravates the chromatic aberration.

Overall, the narrowband PBLs were successfully fabricated, and their performance in the achromatic PBL system was also experimentally validated using a laser projector. However, due to the limited thickness and birefringence of RM257, the theoretical contrast ratio (C_R, C_G, and C_B) for the RGB colors, based on the spectra in Fig. 2(a–c), are only around 50∶1 if the contrast ratio, using the red PBL as an example, is defined as follows:

$$C_R = \frac{E_R}{E_G + E_B}, \tag{6}$$

where E_R, E_G, and E_B denotes the diffraction efficiency of the RGB lights in the red PBL, respectively. Therefore, to fully explore the potential of the multi-twist structure

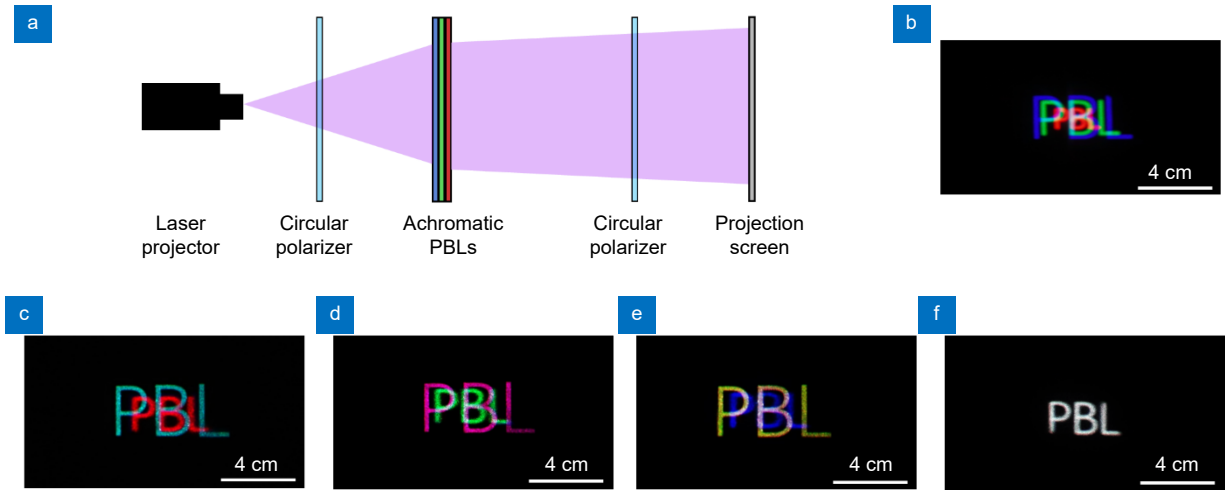

Fig. 5 | Achromatic imaging experiments with a laser projector. (**a**) Optical setup for the imaging process with a laser projector. Image on the projection screen with (**b**) a broadband PBL, (**c**) a red PBL, (**d**) a green PBL, (**e**) a blue PBL, and (**f**) the stacked achromatic PBLs.

for designing narrowband PBOEs and achieving an achromatic PBOE, we first optimized a set of thicker narrowband PBOE with RM 257 to achieve a contrast ratio of over 500∶1 for the RGB wavelengths at 464.5 nm, 527 nm, and 633 nm. It should be mentioned that there is no limitation on the choice of RGB wavelengths and birefringence dispersion of the LC materials. As shown in Fig. 6(a–c), the spectra of the three PBOEs with high contrast ratio were simulated with and RCWA model[33], and their twisting angles and thicknesses are listed in Table 4. Additionally, the angular response is shown in Fig. 6(d–f). Although the optimization is performed at normal incidence, the PBDs can still achieve over 95% efficiency for angles up to ±15°, making them suitable for collimated LED sources or other VR/AR light engines. Future optimizations will incorporate angular response depending on the specific application requirements.

Next, we perform polarization raytracing simulations using OpticStudio (Ansys Zemax) to further investigate the optical performance of the achromatic PBOE system with laser sources, LED sources, and quantum dot color conversion layer. Taking the PB deflector (PBD) or grating

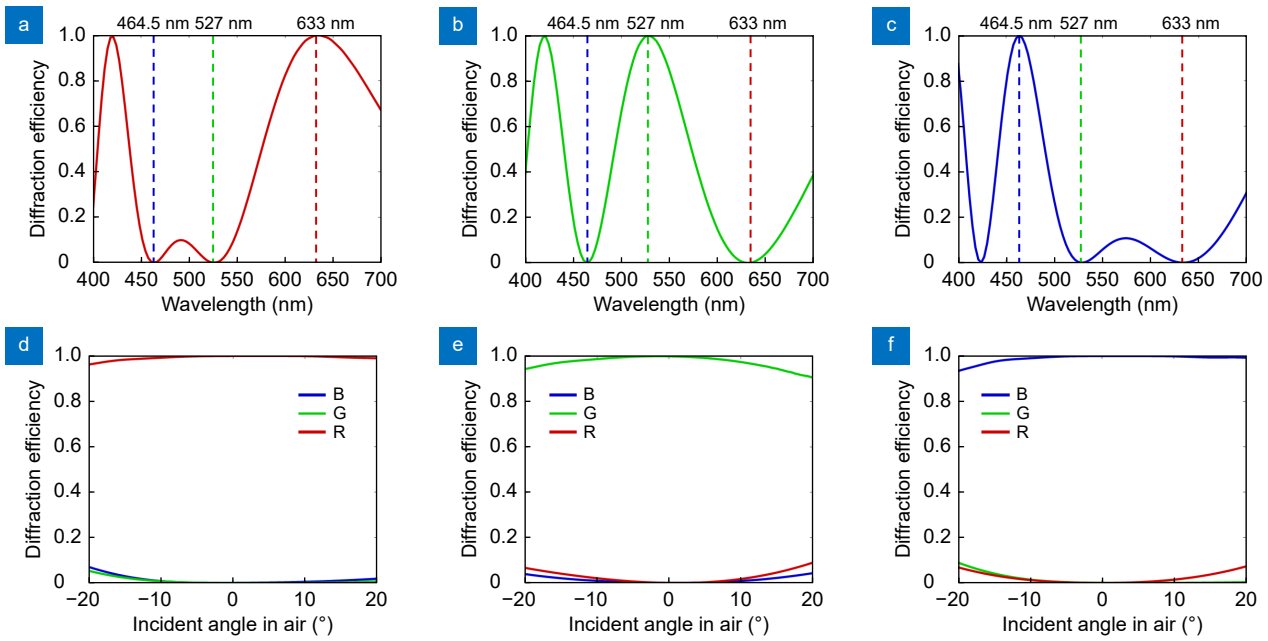

Fig. 6 | Spectral response of the designed narrowband PBLs with high contrast ratio. Spectra of **(a)** the red PBL, **(b)** the green PBL, and **(c)** the blue PBL with RCWA simulations. Simulated angular response of **(d)** the red PBL, **(e)** the green PBL, and **(f)** the blue PBL. The employed RGB wavelengths are *R*=633 nm, *G*=527 nm, and *B*=464.5 nm.

as an example, the RCWA model of PBD, a part of PBL, was compiled into a dynamic-link library (DLL) file and linked to OpticStudio, operating in non-sequential mode. During the raytracing process in OpticStudio, if a ray hits the PBD with a DLL, RCWA is automatically called to solve the field response and provide return data. The mathematical construction process is detailed in our previous publications[34,35]. To simplify the comparison of chromatic aberration correction among laser sources, LED sources, and quantum dot color conversion layer, we use the central wavelength of B=464.5 nm, G=527 nm, and R=633 nm from the LEDs by Nichia for all three types of light sources. To achieve D65 white light with RGB laser wavelengths of 464.5 nm, 527 nm, and 633 nm, the power ratio is set as 1 ∶ 1.22 ∶ 1.70 in OpticStudio as shown in Fig. 7(a). After stacking three narrowband PBDs with the parameters shown in Table 4, the horizontal periods ($\Lambda_{x\mathrm{R}}$, $\Lambda_{x\mathrm{G}}$, and $\Lambda_{x\mathrm{B}}$) of RGB PBDs should satisfy the following relationship to eliminate or mitigate the chromatic aberration.

$$\frac{\lambda_{\mathrm{R}}}{\Lambda_{x\mathrm{R}}}=\frac{\lambda_{\mathrm{G}}}{\Lambda_{x\mathrm{G}}}=\frac{\lambda_{\mathrm{B}}}{\Lambda_{x\mathrm{B}}}. \tag{7}$$

Therefore, if the horizontal period of green light is set as 6500 nm, then the horizontal period of the blue and red lights should be 5729.1 nm and 7807.4 nm, respectively. After polarization raytracing in Zemax, as depicted in Fig. 7(b), the chromatic aberration is indeed eliminated with these three narrowband PBDs, compared to the chromatic aberration in a broadband PBD with a horizontal period of 6500 nm as shown in Fig. 7(c).

To further investigate the chromatic correction in the PBDs system for RGB light sources with a certain bandwidth, we applied LEDs (Nichia STS-DA1-5909) with spectrum shown in Fig. 7(d) in OpticStudio, while keeping the rest of the setup unchanged. As shown in Fig. 7(e), the chromatic aberration is significantly reduced as compared to that of a broadband PBD with a horizontal period of 6500 nm, as depicted in Fig. 7(f). However, there remains a weak chromatic aberration in Fig. 7(e) when using the LED light sources with a certain

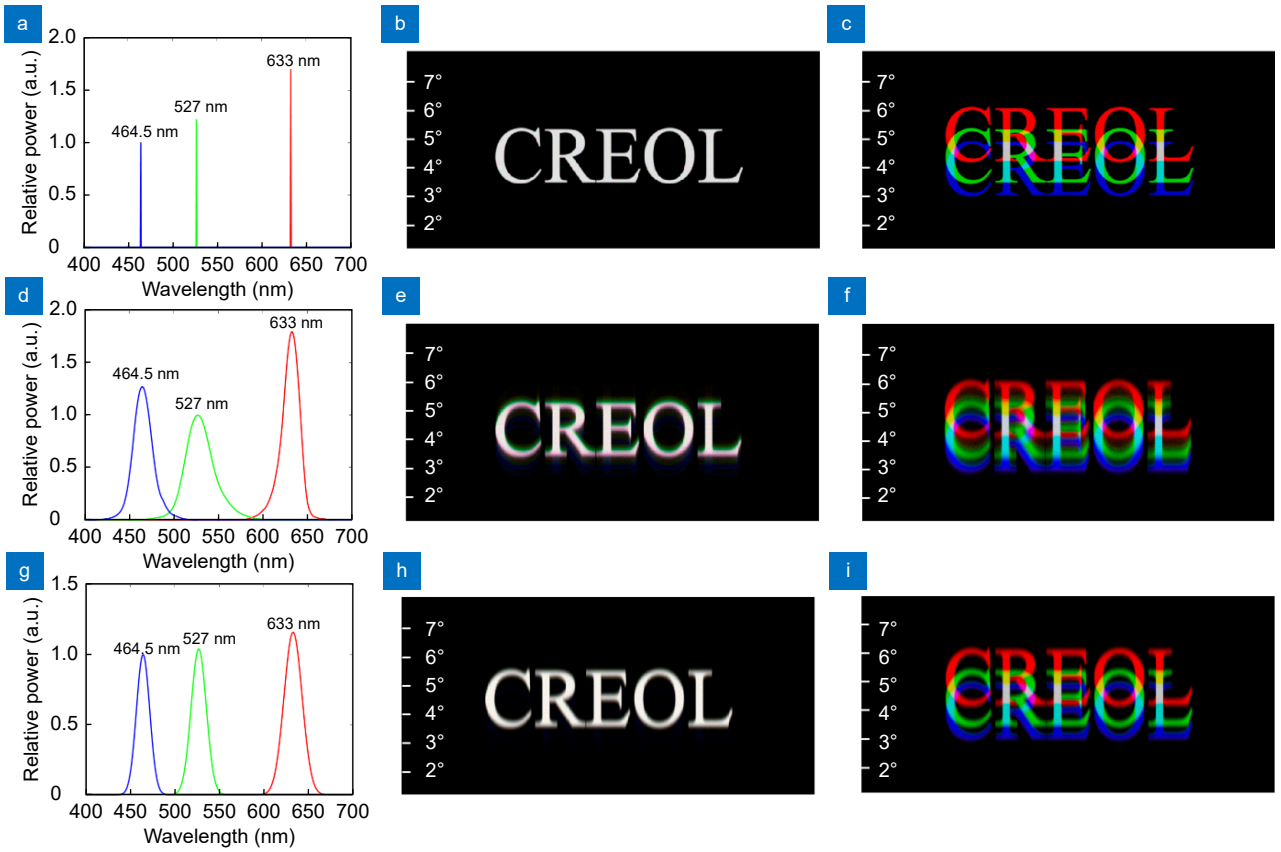

Fig. 7 | Polarization raytracing of an achromatic PBD using three narrowband PBDs with high contrast ratios. (**a**) Spectrum of an RGB laser projector. (**b**) Image in an achromatic PBD system with the laser projector. (**c**) Image with a broadband PBD system using a laser projector. (**d**) Spectrum of the RGB LED light source. (**e**) Image with a nearly achromatic PBD system using the LED light source. (**f**) Image with a broadband PBD system using the LED light source. (**g**) Spectrum of the RGB QD LEDs. (**h**) Image with a nearly achromatic PBD system using the RGB QD LEDs. (**i**) Image with a broadband PBD system using the RGB QD LEDs.

Table 4 | Parameters of the RGB narrowband PBLs with a contrast ratio of 500:1.

	B PBL		G PBL		R PBL	
Layer	d_i (nm)	α_i (°)	d_i (nm)	α_i (°)	d_i (nm)	α_i (°)
1st	1772.9	−13.02	1471.5	13.98	1563.6	−33.39
2nd	1911.7	47.17	1670.4	44.09	2578.3	2.25
3rd	1664.1	−3.95	1102.0	32.45	1491.5	60.22
4th	1782.2	24.39	1637.2	25.37	2548.2	−21.51
5th	1885.5	−26.21	1862.9	7.95	1580.2	−39.45

bandwidth (20–40 nm), despite the high contrast ratio and well-optimized spectral bandwidth of the narrowband PBOEs. This slight chromatic aberration essentially arises from the chromatic correction method, which only addresses the chromatic aberration for three specific RGB wavelengths with three narrowband PBOEs. Within each narrowband PBOE, such as a green PBL, a weak chromatic aberration is still noticeable because of the 40 nm bandwidth of the green LEDs. However, a narrower spectrum RGB sources can further suppress such chromatic aberration. For example, using QD LEDs with 20 nm FWHM as shown in Fig. 7(g), the chromatic aberration can be suppressed based on the polarization raytracing in Fig. 7(h-i).

It should be noted that our method can be easily applied to other achromatic systems[14,15,17,18] that rely on narrowband HWPs or PBOEs with any phase profile. By using our narrowband PBOEs or HWPs, the optical efficiency in these achromatic systems could achieve nearly 100%, which helps to significantly suppress the stray lights and ghost images. In addition, the wavelength choice of the light source will not be limited by the LC materials, which will greatly increase the degree of design freedom.

The LC parameters used in our optimized narrowband PBLs and PBDs can be extended to other patterns or holograms with a relatively slow varying phase profile. However, as the phase variation increases, such as a shorter pitch of the PBD or a lower *f*/# of the PBL, the gratings are gradually close to Bragg region, which require a strong phase matching among the input light, grating, and output light, thus the angular response shifts away from normal incidence[28,36,37], resulting in a deviation from the designed spectrum. More importantly, for a short-pitch PBD, the angular response can be easily shifted back to normal incidence by optimizing our multi-twist structure because the Bragg angle in each layer of PBOEs can be optimized to realize the phase matching. In contrast, for a low *f*/# PBL, which acts as a spatially gradient PBD, the response will vary at different positions, requiring optimization based on the local grating pitch. Therefore, low *f*/# PBLs may necessitate using inkjet printing[38] instead of the spin-coating method for device fabrication. In the future, developing a DLL for PBLs will be essential for further studying their angular performance.

Additionally, our approach offers a simpler fabrication process and higher tolerance in comparison with previous methods[15], because it requires a much thinner film (about 3 to 4 times smaller phase retardation). Using a higher birefringence LC material, the thickness can be further reduced, which makes the device fabrication simpler and molecular alignment better, thus achieving a higher contrast ratio. More specifically, the narrowband performance of PBOEs is closely linked to the thickness of each layer. Thus, making careful consideration of the PBOE surface flatness during fabrication is essential. Using spin-coating, surface flatness may vary across layers. After multiple spin-coating processes, the fabricated thickness and twist angles of each layer may significantly deviate from the target, causing severe spectral mismatches with the simulation results. This deviation could be more pronounced as the total layer thickness increases. Although our method can achieve high-performance narrowband PBOEs with a thinner layer thickness, further investigation on improving surface flatness during the fabrication of LC-based PBOEs using spin-coating, inkjet printing[39], or other technologies would be useful.

Essentially, all current methods can theoretically eliminate the chromatic aberration in LC-based PBOEs for RGB laser sources. However, for QD LED light sources with 20-nm FWHM, a nearly achromatic behavior can be achieved as simulated in Fig. 7(h). To achieve truly achromatic PBOEs without any chromatic aberration for LED light engines, new approaches remain to be explored.

Conclusions

We have discovered and demonstrated a novel

method using the multi-twist structure for achieving narrowband PBOEs without crosstalk and realizing high-efficiency achromatic PBOEs while maintaining a compact formfactor. As demonstrated through our experiments and polarization raytracing, this method can effectively eliminate the chromatic aberration of the PBOEs using a laser projector. On the other hand, if a QD LED light source with 20 nm FWHM is employed, a nearly achromatic behavior can still be achieved. To further explore the potential of multi-twist structure, narrowband PBOEs with a contrast ratio of over 500∶1 are designed and investigated. Importantly, this method does not constrain the choice of RGB wavelengths or the birefringence dispersion of liquid crystal materials, thus offering a high degree of design freedom for different light sources and liquid crystal materials. Overall, these demonstrations showcase that our proposed method exhibits a high optical efficiency, low fabrication complexity, and extensive design freedom for any liquid crystal material and RGB light sources, holding immense potential for widespread applications of PBOEs.

References

1. Xiong JH, Hsiang EL, He ZQ et al. Augmented reality and virtual reality displays: emerging technologies and future perspectives. *Light Sci Appl* **10**, 216 (2021).
2. Kress BC. *Optical Architectures for Augmented-, Virtual-, and Mixed-Reality Headsets* (Bellingham: SPIE, 2020).
3. Ding YQ, Yang Q, Li YNQ et al. Waveguide-based augmented reality displays: perspectives and challenges. *eLight* **3**, 24 (2023).
4. Yang ZY, Luo ZY, Ding YQ et al. Advances and challenges in microdisplays and imaging optics for virtual reality and mixed reality. *Device* **2**, 100398 (2024).
5. Li Y, Huang X, Liu SX et al. Metasurfaces for near-eye display applications. *Opto-Electron Sci* **2**, 230025 (2023).
6. Chen P, Wei BY, Hu W et al. Liquid-crystal-mediated geometric phase: from transmissive to broadband reflective planar optics. *Adv Mater* **32**, 1903665 (2020).
7. Yin K, Hsiang EL, Zou JY et al. Advanced liquid crystal devices for augmented reality and virtual reality displays: principles and applications. *Light Sci Appl* **11**, 161 (2022).
8. Zhan T, Zou JY, Xiong JH et al. Practical chromatic aberration correction in virtual reality displays enabled by cost-effective ultra-broadband liquid crystal polymer lenses. *Adv Opt Mater* **8**, 1901360 (2020).
9. Wang P, Mohammad N, Menon R. Chromatic-aberration-corrected diffractive lenses for ultra-broadband focusing. *Sci Rep* **6**, 21545 (2016).
10. Evdokimova VV, Podlipnov VV, Ivliev NA et al. Hybrid refractive-diffractive lens with reduced chromatic and geometric aberrations and learned image reconstruction. *Sensors* **23**, 415 (2023).
11. Mo ZC, Zhao YN, Wang JG et al. Intensity-tunable achromatic cascade liquid crystal Pancharatnam-Berry lens. *Commun Phys* **7**, 113 (2024).
12. Millán MS, Otón J, Pérez-Cabré E. Dynamic compensation of chromatic aberration in a programmable diffractive lens. *Opt Express* **14**, 9103–9112 (2006).
13. Brown DC. Decentering distortion of lenses. *Photogramm Eng* **32**, 444–462 (1996).
14. Lu L, Lam WST, McEldowney SC et al. Apochromatic pancharatnam berry phase (PBP) liquid crystal structures for head-mounted displays. US10705401B1 (2020-07-07).
15. Li LS, Shi SJ, Kim J et al. Color-selective geometric-phase lenses for focusing and imaging based on liquid crystal polymer films. *Opt Express* **30**, 2487–2502 (2022).
16. Zhang DW, Xu CT, Chen QM et al. Cascaded chiral birefringent media enabled planar lens with programable chromatic aberration. *PhotoniX* **5**, 17 (2024).
17. Luo ZY, Li YNQ, Semmen J et al. Achromatic diffractive liquid-crystal optics for virtual reality displays. *Light Sci Appl* **12**, 230 (2023).
18. Huang YG, Lu L, Diorio N et al. 60–3: *Invited Paper*: liquid crystal optics for AR/VR/MR near eye displays. *SID Symp Dig Tech Papers* **54**, 857–860 (2023).
19. Moon S, Lee CK, Nam SW et al. Augmented reality near-eye display using Pancharatnam-Berry phase lenses. *Sci Rep* **9**, 6616 (2019).
20. Wu ST. Birefringence dispersions of liquid crystals. *Phys Rev A* **33**, 1270–1274 (1986).
21. Evans JW. Solc birefringent filter. *J Opt Soc Am* **48**, 142–145 (1958).
22. Li LS, Shi SJ, Escuti MJ. Improved saturation and wide-viewing angle color filters based on multi-twist retarders. *Opt Express* **29**, 4124–4138 (2021).
23. Oh C, Escuti MJ. Achromatic diffraction from polarization gratings with high efficiency. *Opt Lett* **33**, 2287–2289 (2008).
24. Momosaki R, Ashikawa K, Sakamoto M et al. Incident angle dependence-reduced polarization grating performance by using optically biaxial polymer liquid crystal. *Opt Lett* **44**, 5929–5932 (2019).
25. Zou JY, Zhan T, Xiong JH et al. Broadband wide-view Pancharatnam–Berry phase deflector. *Opt Express* **28**, 4921–4927 (2020).
26. Chen W, Yu Y, Mu QQ et al. Super-broadband geometric phase devices based on circular polarization converter with mirror symmetry. *Appl Phys Lett* **119**, 101103 (2021).
27. Komanduri RK, Lawler KF, Escuti MJ. Multi-twist retarders: broadband retardation control using self-aligning reactive liquid crystal layers. *Opt Express* **21**, 404–420 (2013).
28. Gao K, McGinty C, Payson H et al. High-efficiency large-angle Pancharatnam phase deflector based on dual-twist design. *Opt Express* **25**, 6283–6293 (2017).
29. Pancharatnam S. Generalized theory of interference, and its applications. *Proc Indian Acad Sci A* **44**, 247–262 (1956).
30. Berry MV. Quantal phase factors accompanying adiabatic changes. *Proc Roy Soc A: Math Phys Sci* **392**, 45–57 (1984).
31. Xiong JH, Wu ST. Planar liquid crystal polarization optics for augmented reality and virtual reality: from fundamentals to applications. *eLight* **1**, 3 (2021).
32. Kim J, Li YM, Miskiewicz MN et al. Fabrication of ideal geometric-phase holograms with arbitrary wavefronts. *Optica* **2**, 958–964 (2015).

33. Xiang X, Escuti MJ. Numerical modeling of polarization gratings by rigorous coupled wave analysis. *Proc SPIE* **9769**, 976918 (2016).
34. Ding YQ, Li YNQ, Yang Q et al. Design optimization of polarization volume gratings for full-color waveguide-based augmented reality displays. *J Soc Inf Disp* **31**, 380–386 (2023).
35. Wei R, Liu HT, Weng YS et al. Realizing the imaging simulation of reflective polarization volume gratings. *Opt Express* **30**, 6355–6364 (2022).
36. Xi FL, Bos P. Intuitive understanding of the connection between Pancharatnam–Berry optical beam deflectors and polarization volume holograms. *Appl Opt* **62**, 1845–1852 (2023).
37. Gao K, Cheng HH, Bhowmik AK et al. Thin-film Pancharatnam lens with low f-number and high quality. *Opt Express* **23**, 26086–26094 (2015).
38. Yang X, Lin Y, Wu TZ et al. An overview on the principle of inkjet printing technique and its application in micro-display for augmented/virtual realities. *Opto-Electron Adv* **5**, 210123 (2022).
39. Xiong JH, Zhong HZ, Cheng DW, et al. Full degree-of-freedom polarization hologram by freeform exposure and inkjet printing. *PhotoniX* **4**, 35 (2023).

Acknowledgements

The UCF group is grateful to John Semmen for technical assistance. The SJTU group is indebted to the financial supports from the National Key Research and Development Program of China (2023YFB2806803) and the National Natural Science Foundation of China (62075127).

Author contributions

Y. Q. Ding proposed the idea and initiated the project. Y. Q. Ding and X. J. Huang mainly conducted the experiments and simulations and wrote the manuscript. Y. Z. Y. Ma helped with experiments. S.-T. Wu and Y. Li supervised the project and edited the manuscript.

Competing interests

The authors declare no competing financial interests.